Enhanced theoretical framework for bilayer stacking ferroelectricity

Jiaqi Xin [1,2] Yaguang Guo [1,2,*] and Qian Wang [3]

[1] *Department of Physics, School of Physical Science and Engineering, Beijing Jiaotong University, Beijing 100044, China*

[2] *Beijing Key Laboratory of Novel Materials Genetic Engineering and Application for Rail Transit, Beijing Jiaotong University, Beijing 100044, China*

[3] *School of Materials Science and Engineering, Peking University, Beijing 100871, China*

(Received 7 March 2025; revised 23 May 2025; accepted 28 May 2025; published 6 June 2025)

Sliding ferroelectricity has garnered significant research interest in recent years, and the foundational bilayer stacking ferroelectricity (BSF) theory [Ji *et al.*, Phys. Rev. Lett. **130**, 146801 (2023)] provides valuable guidelines for the design of sliding ferroelectrics. However, the current framework does not fully account for the selection of rotation operators in bilayer stacking, and is unable to determine whether and how the direction of polarization can be switched in polar bilayers. Here, we introduce two key improvements to the BSF theory through a systematic group theory analysis. First, we develop a more general method for identifying possible rotation operators, enabling a refined classification of the symmetries and polar states in bilayers that arise when stacking monolayers from oblique and rectangular crystal systems. Second, we establish an approach to determine the symmetry operators that connect the energetically degenerate configurations, thereby integrating the determination of ferroelectric switching into the BSF theory. These enhancements make the theory more comprehensive, providing a more robust and practical foundation for the design of sliding ferroelectrics.

DOI: 10.1103/PhysRevB.111.224102

I. INTRODUCTION

Ferroelectric crystals exhibit switchable spontaneous polarization in response to an electric field. Recent advances in achieving ferroelectricity in two dimensional (2D) materials, such as $CuInP_2S_6$ [1,2], α-In_2Se_3 [3–5], α-Bi [6], and $MoTe_2$ [7] monolayers, have inspired widespread exploration of nonvolatile memory [8,9], photovoltaics [10–14], and other applications at nanoscales. However, because ferroelectricity requires the system to have noncentrosymmetric configuration, excluding a large portion of known materials, the number of 2D ferroelectrics discovered to date is very limited.

In 2017, Li *et al.* proposed the concept of sliding ferroelectricity, offering a promising strategy to engineer bilayer ferroelectrics from nonpolar monolayers [15]. In this scheme, the spontaneous polarization occurs at the interface due to a specific stacking sequence that breaks the symmetry under appropriate conditions. Such a phenomenon has been experimentally observed in multiple bilayer systems, including BN [16–18], transition metal dichalcogenides (TMDs) [19–23], and γ-InSe [24,25]. Theoretically, Ji *et al.* further developed a bilayer stacking ferroelectricity (BSF) theory, which addresses how polar states are induced by stacking two monolayers with misalignments between their crystal structures [26]. The BSF theory provides a unified group theory framework that encompasses all types of monolayers and the possible types of stacking configurations, including rotations and translations. It not only provides a clear understanding for some known sliding ferroelectrics like BN and MoS_2, but also guides the prediction of a series of different polar bilayer materials [10,27–34].

However, the BSF theory needs further refinement for the following two reasons. First, we found that the BSF theory is not fully applicable to all materials. A notable example is 2D $LiAuI_4$, which is a van der Waals (vdW) layered material included in the MC2D database [35]. As shown in Fig. 1(a), monolayer $LiAuI_4$ belongs to the layer group (LG) of $P\bar{1}$ (no. 2) and point group (PG) of C_i. According to the BSF theory, when 2D materials with this symmetry are stacked into a bilayer, it is supposed to exhibit one of three types of PG symmetries, i.e., C_i, C_s, and C_1 [see the blue region in the inset table of Fig. 1(a)]. However, when a bilayer is formed via direct exfoliation from the bulk phase of $LiAuI_4$, it exhibits C_2 symmetry instead. Such discrepancy implies that the current BSF theory is incomplete. Second, not all bilayers with spontaneous polarization can be classified as ferroelectrics. For instance, bilayer pentagonal $PdSe_2$ exhibits the C_{2v} symmetry with in-plane polarization [36]. Nevertheless, this polar state corresponds to only one ground-state stacking configuration [Fig. 1(b)], which means that it is impossible to find another energetically degenerate configuration with a different direction of polarization via sliding. The current BSF theory determines whether a bilayer structure exhibits polarization, namely, addresses only the "electricity" aspect of "ferroelectricity." It does not assess whether the polarization direction is switchable, leaving the "ferro" aspect, which is crucial for applications such as sensor, and information storage, unexamined. As a result, density functional theory (DFT) calculations

*Contact author: ygguo@bjtu.edu.cn

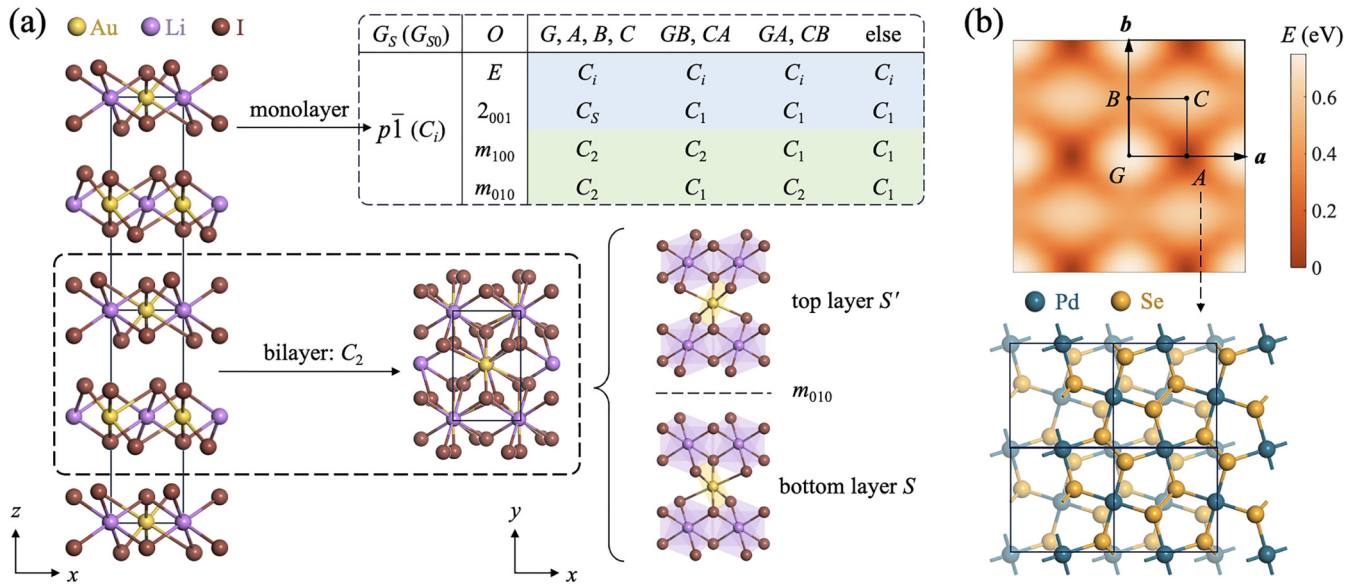

G_S (G_{S0})	O	G, A, B, C	GB, CA	GA, CB	else
$p\bar{1}$ (C_i)	E	C_i	C_i	C_i	C_i
	2_{001}	C_S	C_1	C_1	C_1
	m_{100}	C_2	C_2	C_1	C_1
	m_{010}	C_2	C_1	C_2	C_1

FIG. 1. (a) Left: side view of the bulk $LiAuI_4$. The exfoliated monolayer belongs to the PG of C_i, while the bilayer exhibits the C_2 symmetry. The bilayer has a rectangular lattice with its top and bottom layers connected by the mirror plane m_{010}. Blue region: all possible bilayer symmetries predicted by the original BSF theory. Green region: additional bilayer symmetries from the improved theory. (b) Top: calculated energy distribution of the bilayer $PdSe_2$ with different interlayer translations. Bottom: top view of the unique ground-state stacking configuration at translation point A.

are still needed to determine whether a polar bilayer structure is ferroelectric.

In this work, we first demonstrate the limitations of the BSF theory arising from the insufficient selection of rotation operators in bilayer stacking, and then propose a more general method for determining possible types of rotation operators in bilayer stacking with unchanged cell size. Using this approach, we revisit the BSF framework for 2D materials belonging to oblique and rectangular crystal systems, and show that bilayer stacking can exhibit more diverse polar states as compared to the original theory. We further extend the theory on determining whether the polar bilayers can exhibit ferroelectricity and how the direction of polarization switches among the energetically degenerate configurations by solving the symmetry relationships among the sliding vectors. The improved BSF theory is more general and more efficient for the design of bilayer sliding ferroelectrics.

II. COMPUTATIONAL DETAILS

Energy distribution of bilayer $PdSe_2$ for different interlayer translations were calculated by using density functional theory within the Vienna *Ab Initio* Simulation Package [37] and the projector augmented wave method [38]. The Perdew-Burke-Ernzerhof functional within the generalized gradient approximation [39] was employed to describe the electronic exchange-correlation interactions. A plane-wave energy cutoff of 500 eV was used, and the Monkhorst-Pack k-point mesh was sampled with a density of $2\pi \times 0.01$ Å^{-1} [40]. Full structural optimization was carried out with convergence criteria of 0.01 eVÅ^{-1} for atomic forces and 1×10^{-4} eV for total energy. To eliminate spurious interactions between periodic images, a vacuum layer of 15 Å was introduced along the nonperiodic direction. van der Waals interactions were accounted for using the DFT-D3 correction method.

III. RESULTS AND DISCUSSION

A. Improvement 1: Selection of rotation operators for bilayer stacking

In this section, the original BSF framework is first introduced, followed by a clarification of 2D crystal systems and lattice systems to illustrate its limitation. Then, we propose a more general method for determining possible rotation operators. By using this method, the symmetries and polar types of the bilayer formed by stacking monolayers belonging to oblique and rectangular crystal systems are resummarized.

1. Limitations of the original BSF theory

According to the BSF theory [26], a 2D monolayer is denoted as S with its corresponding PG and LG represented by G_{S0} and G_S, respectively. A bilayer (B) system formed from S is denoted as $B = S + S'$, where S' is obtained by applying a stacking operator $\hat{\tau}_z\hat{O}$ on S. $\hat{O} = \{O|\tau_O\}$ consists of a rotation operator O and an in-plane translation operator τ_O, while $\hat{\tau}_z = \{E|\tau_z\}$ is an out-of-plane translation operator that does not affect the symmetry of B. Therefore, once G_S, O, and τ_O are known, the symmetry and polar type of B are determined. Based on this framework, the BSF theory explores all possible polar types of the bilayers formed from monolayers belonging to all 80 LGs.

Note that, to enhance the polarization of stacked bilayers, the BSF theory focuses on the bilayer structures without expanding the cell size, i.e., S and B share identical lattice vectors. In this case, the possible rotation operators O are derived from the distinct coset representatives of

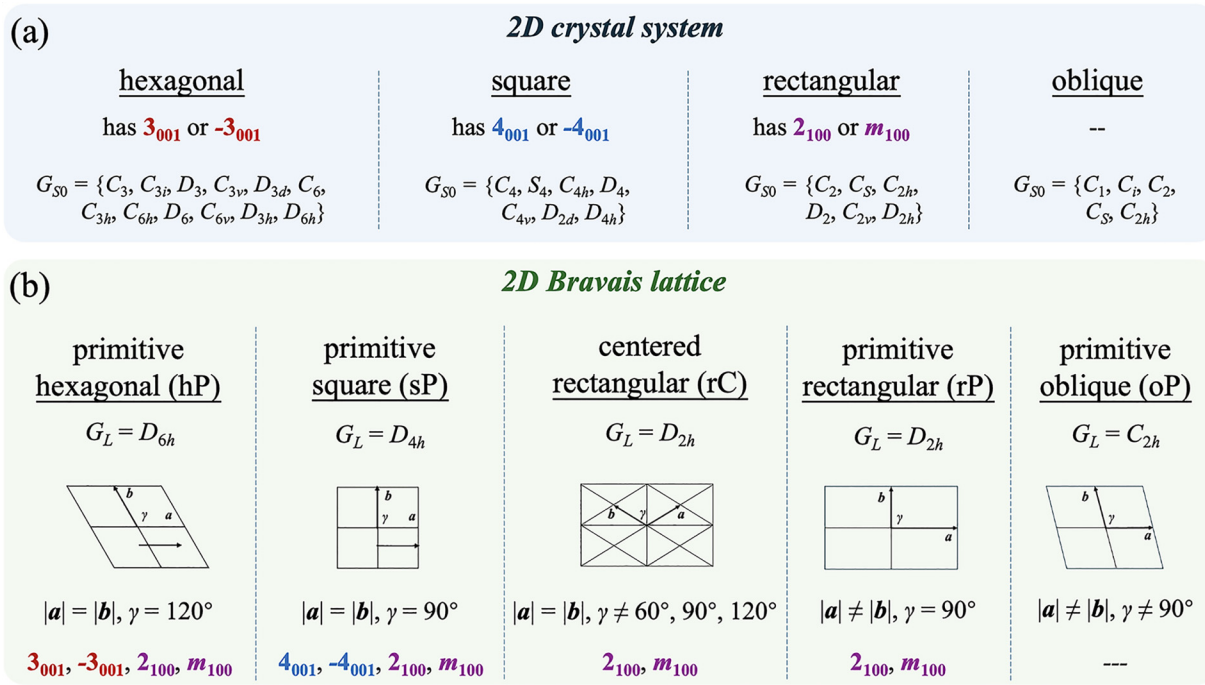

FIG. 2. (a) 2D crystal system, classified based on the rotation or improper rotation in the PG of the material. (b) 2D Bravais lattice, defined by the lattice shape.

the factor group G_L/G_{S0}, where G_L represents the PG of the Bravais lattice of S. For example, in rectangular $1T'$-WTe_2 [23,41,42], $G_{S0} = C_{2h} = \{E, m_{100}, I, 2_{100}\}$, and $G_L = D_{2h} = \{E, I, 2_{001}, 2_{010}, 2_{100}, m_{100}, m_{010}, m_{001}\}$, where E represents the identity operator, I denotes the inversion operator, and other symmetry operators follow Seitz notation [43] (see Sec. I of the Supplemental Material [44]). This yields $G_L/G_{S0} = \{\{E, m_{100}, I, 2_{100}\}, \{m_{001}, 2_{001}, m_{010}, 2_{010}\}\}$. Therefore, one can choose the representative element E or m_{001} as O forming two distinct stacked bilayers while maintaining the cell size unchanged. Next, we show that this method cannot give all possible O for some LGs due to the distinction of the crystal system and the lattice system, hence resulting in the limitations of the original theory.

2D materials may have finite thickness along the nonperiodic direction, thus G_{S0} is one of the 27 PGs of three dimensions, excluding T, T_h, O, T_d, and O_h [45]. 2D materials with these 27 PGs are classified into four crystal systems based on symmetry characteristics [Fig. 2(a)]: those with 3_{001} or -3_{001} belong to the hexagonal crystal system; those with 4_{001} or -4_{001} belong to the square crystal system; those lacking these symmetries but featuring 2_{100} or m_{100} belong to the rectangular crystal system; and all others are classified into the oblique crystal system. For monolayer S with a certain PG, its corresponding crystal system can be identified according to such a principle.

Distinct from the crystal system, the lattice system reflects the translational symmetry within the periodic plane [Fig. 2(b)]. There are five types of 2D Bravais lattices, primitive oblique (oP), primitive rectangular (rP), centered rectangular (rC), primitive square (sP), and primitive hexagonal (hP) [46]. They are classified based on the primitive vectors $\boldsymbol{a}$ and $\boldsymbol{b}$ and the angle γ between them. For the hP lattice, the lattice symmetry (G_L) is D_{6h}, which includes 3_{001} and 2_{100}. Therefore, monolayers belonging to the hexagonal, rectangular, and oblique crystal systems can all adopt the hP lattice, while those belonging to the square crystal system cannot, as 4_{001} or -4_{001} are incompatible with the hP lattice symmetry. For the sP lattice, $G_L = D_{4h}$, which includes 4_{001} and 2_{100}. This indicates that monolayers belonging to the square, rectangular, and oblique crystal systems can all adopt the sP lattice, while those from the hexagonal crystal system cannot due to the incompatibility of 3_{001} with the sP lattice symmetry. For a similar reason, monolayers belonging to the oblique crystal system may also adopt the rectangular lattice.

Returning to the example of $LiAuI_4$, monolayer $LiAuI_4$ has the PG symmetry of C_i (i.e., $G_{S0} = C_i$), thus belonging to the oblique crystal system. However, this material possesses a rectangular lattice rather than oblique one, as shown in Fig. 1(a). In the original BSF theory, when a monolayer with PG of C_i is stacked into a bilayer, the rotation operator O is determined by constructing the factor group C_{2h}/C_i, where it implicitly assumes that such a material have an oblique lattice ($G_L = C_{2h}$). However, the real rectangular lattice possesses higher symmetry ($G_L = D_{2h}$), which allows more choices of O for bilayer stacking of $LiAuI_4$, because the factor group $D_{2h}/C_i = \{\{E, I\}, \{2_{001}, m_{001}\}, \{m_{100}, 2_{100}\}, \{m_{010}, 2_{010}\}\}$ contains more elements as compared to $C_{2h}/C_i = \{\{E, I\}, \{2_{001}, m_{001}\}\}$. From Fig. 1(a), one can see that the top and bottom (S' and S) layers of bilayer $LiAuI_4$ are related by the m_{010} mirror plane, a rotation operator O that is excluded in C_{2h}/C_i but included in D_{2h}/C_i.

The above discussion shows that when searching for all possible O, it is supposed to consider the specific lattice type (the minimal 2D Bravais lattice) corresponding to the studied monolayer, because a 2D material belonging to a certain

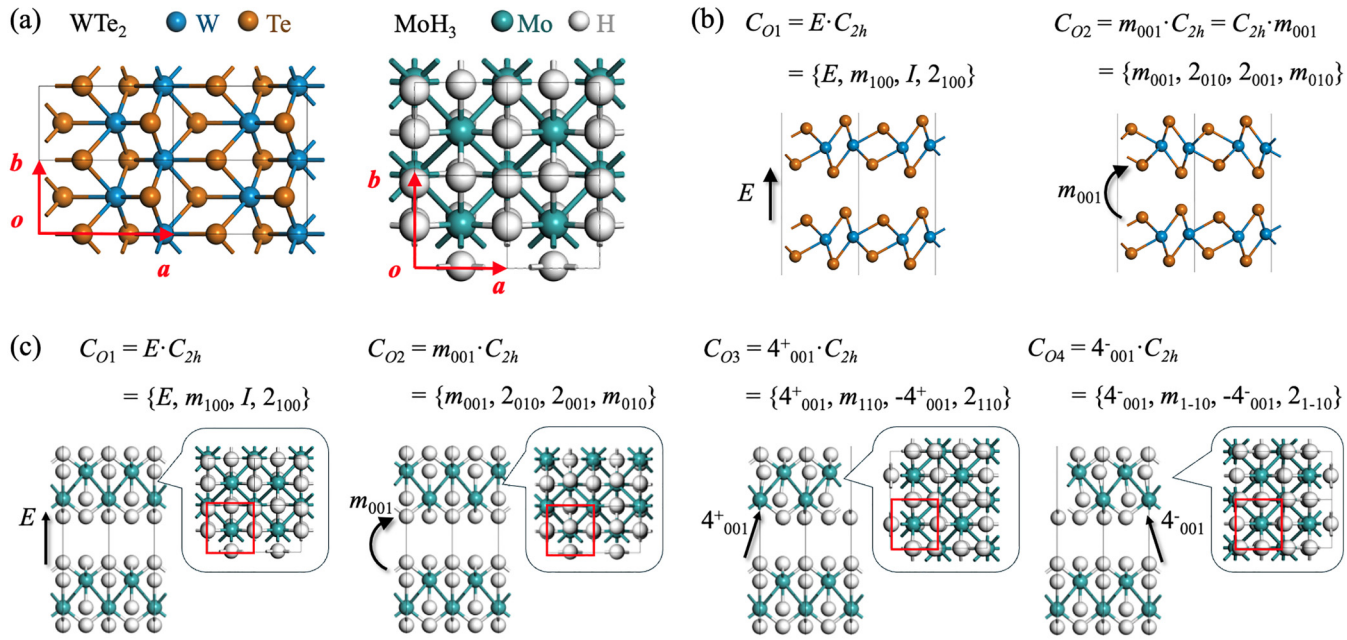

FIG. 3. (a) Top views of monolayer WTe_2 and MoH_3, both with same crystal symmetry but different lattice symmetry. (b) Possible O for WTe_2 bilayer stacking. C_{O1} and C_{O2} are two elements in factor group D_{2h}/C_{2h}. (c) Possible O for MoH_3 bilayer stacking. C_{O1}, C_{O2}, C_{O3}, and C_{O4} are four subsets of D_{4h}, each of which defines a distinct bilayer configuration of MoH_3 as plotted in the corresponding below image.

crystal system does not necessarily mean it has a lattice with the same name. Specifically, for the monolayers belonging to the oblique crystal system (LG-1 to 7), the selection of O should be considered under the rectangular, square, and hexagonal lattices in addition to the oblique one. Similarly, for the monolayers belonging to the rectangular crystal system (LG-8 to 48), one needs to consider the cases under the square and hexagonal lattices apart from the rectangular one; as for the square and hexagonal crystal systems (LG-49 to 80), the monolayers can only adopt the lattice type that shares the same name as their crystal system, because of the high crystal symmetry. Based on this, our first improvement to the BSF theory is to identify all additional symmetry operators for bilayer stacking of 2D materials belonging to oblique and rectangular crystal systems as their lattice symmetry G_L increases.

2. A more general approach in determining the rotation operator O

The construction of factor group G_L/G_{S0} requires that G_{S0} must be an invariant subgroup of G_L. However, as the lattice symmetry increases, G_{S0} may no longer remain an invariant subgroup of G_L, making the method for identifying representative elements in the factor group G_L/G_{S0} not fully applicable. To illustrate this, we present two examples of 2D materials, WTe_2 and MoH_3, as shown in Fig. 3(a). Both monolayers belong to the same symmetry group (i.e., $G_{S0} = C_{2h}$ and G_S = LG-15). Monolayer WTe_2 has a rP lattice [23,41,42], where $G_L = D_{2h}$. Since C_{2h} is an invariant subgroup of D_{2h}, two different types of O (E and m_{001}) that form distinct bilayer WTe_2 configurations can be identified by constructing factor group D_{2h}/C_{2h}, as shown in Fig. 3(b). Monolayer MoH_3 is included in the Computational 2D Materials Database (C2DB) [47]. Its lattice vectors satisfy $\boldsymbol{a} = \boldsymbol{b}$, and $\gamma = 90°$. Thus, 2D MoH_3 has an sP lattice, where $G_L = D_{4h} = \{E, I, 2_{001}, 2_{010}, 2_{100}, 2_{110}, 2_{1-10}, m_{100}, m_{010}, m_{001}, m_{110}, m_{1-10}, 4^{+}_{001}, 4^{-}_{001}, -4^{+}_{001}, -4^{-}_{001}\}$. Now C_{2h} is only a subgroup of D_{4h}, but not an invariant subgroup, as the left and right cosets differ from each other. For example, $4^{+}_{001} \cdot C_{2h} = \{4^{+}_{001}, -4^{+}_{001}, 2_{110}, m_{110}\}$, while $C_{2h} \cdot 4^{+}_{001} = \{4^{+}_{001}, -4^{+}_{001}, 2_{1-10}, m_{1-10}\}$. Consequently, the rotation operators O for MoH_3 cannot be determined through constructing the factor group.

To address this issue, we revisit the physical origin of O. For monolayer MoH_3 denoted as S, any symmetry operator in C_{2h} acted on S is equivalent to the identity operator, i.e., $S = m_{100} \cdot S = I \cdot S = 2_{100} \cdot S$. Thus, applying 4^{+}_{001} to S would yield $4^{+}_{001}S = 4^{+}_{001} \cdot m_{100}S = 4^{+}_{001} \cdot IS = 4^{+}_{001} \cdot 2_{100}S$, which implies that if $O \in 4^{+}_{001}G_{S0}$ (i.e., one of 4^{+}_{001}, -4^{+}_{001}, m_{110}, and 2_{110}), it leads to a 90° counterclockwise rotation of S. By left-multiplying each element of D_{4h} by C_{2h}, the elements of D_{4h} can be partitioned into four subsets: C_{O1} to C_{O4}, as shown in Fig. 3(c). Specifically, $C_{O1} = C_{2h}$, while C_{O2}, C_{O3}, and C_{O4} correspond to the three distinct left cosets of D_{4h}. Each subset represents a distinct type of rotation. Consequently, four different bilayer configurations of MoH_3 can be constructed. This process provides a more general method for determining O in bilayer stacking across all 80 LGs. One can classify the elements in G_L by determining the left cosets of G_{S0}, which might be more convenient than constructing the factor group.

By applying this approach, we have reidentified all the rotation operators for the 2D materials belonging to oblique and rectangular crystal systems. Based on it, the bilayer symmetry and polar types are also resummarized. Detailed results are presented in Sec. III of the Supplemental Material [44]. Since there are more options when choosing O, bilayers can exhibit more diverse polar states, e.g., 2D $LiAuI_4$ (see Sec. IV of

TABLE I. Polar types of the bilayers formed by stacking two monolayers. Polarization types of the monolayers (P_S) and bilayers (P_B) include OP, IP, CP, and NP. The cases that have changed compared to the original theory are underlined.

P_S		IP	OP		CP
G_S (G_{S0})		4 ∼ 5 (C_S) 8 ∼ 10 (C_2) 27 ∼ 36 (C_{2v})	26 (C_{2v}), 55 ∼ 56 (C_{4v}) 77 (C_{6v})	<u>3 (C_2)</u>, <u>23 ∼ 25 (C_{2v})</u>, 49 (C_4) 65 (C_3), 69 ∼ 70 (C_{3v}), 73 (C_6)	1 (C_1) 11 ∼ 13 (C_S)
P_B	IP	√	×	√	√
	OP	×	√	√	×
	CP	√	√	√	√
	NP	√	√	√	√
P_S		NP			
G_S (G_{S0})		47 ∼ 48 (D_{2h}) 61 ∼ 64 (D_{4h}) 80 (D_{6h})	2 (C_i), 14 ∼ 18 (C_{2h}), 51 ∼ 52 (C_{4h}) 53 ∼ 54 (D_4), 57 ∼ 58 (D_{2d}), 71 (D_{3d}) 75 (C_{6h}), 76 (D_6), 79 (D_{3h})	<u>6 ∼ 7 (C_{2h})</u>, <u>19 ∼ 21 (D_2)</u>, 22 (D_2) <u>37 ∼ 46 (D_{2h})</u>, 50 (S_4), 59 ∼ 60 (D_{2d}) 66 (C_{3i}), 67 ∼ 68 (D_3), 72 (D_{3d}) 74 (C_{3h}), 78 (D_{3h})	
P_B	IP	×	√	√	
	OP	×	×	√	
	CP	×	√	√	
	NP	√	√	√	

the Supplemental Material [44]). In particular, when stacking monolayers belonging to LG-6, 7, 37 to 46, the original BSF theory dictates that the lattice symmetry aligns with crystal symmetry, resulting in the conserved inversion symmetry with nonpolar (NP) state in all their stacked bilayers. However, the improved theory shows that when these monolayers adopt higher-symmetry lattices, their bilayers may exhibit all polar types, including in-plane polarization (IP), out-of-plane polarization (OP), and combined polarization (CP). The possible polar types of the bilayer obtained by stacking two monolayers are summarized in Table I, where the cases that differ from the original theory are highlighted with underlines.

B. Improvement 2: Ferroelectric switching behavior in stacked polar bilayers

Now we focus on the study of the "ferro" aspect of the stacking ferroelectricity. We first present a group theory analysis for symmetry relationships between polar bilayers. Based on it, we develop a workflow to identify the ferroelectric switching behaviors for all 80 LGs.

1. General formalism

Consider two bilayers, $B_1 = S + S_1$ and $B_2 = S + S_2$, where the top layers S_1 and S_2 are generated by applying stacking operators $\hat{\tau}_{z1}\hat{O}_1$ and $\hat{\tau}_{z2}\hat{O}_2$ acting on the bottom layer S, respectively, as plotted in Fig. 4(a). Note that the origin of the coordinate system $\boldsymbol{o}$ is set on the bottom layer S. Because the stable polar states in sliding ferroelectrics are switched via interlayer transition, $\tau_{z1} = \tau_{z2} = \tau_z$ and $O_1 = O_2 = O$, but $\tau_{O1} \neq \tau_{O2}$. In such case, S_1 and S_2 can be expressed as

$$S_1 = \hat{\tau}_{z1}\hat{O}_1 S = OS + \tau_{O1} + \tau_z$$
$$S_2 = \hat{\tau}_{z2}\hat{O}_2 S = OS + \tau_{O2} + \tau_z. \quad (1)$$

The symmetry operator connecting B_1 and B_2 determines how electric polarization switches. For example, the bilayer 1T'-WTe_2 exhibits sliding ferroelectricity with a reversal of OP because the two polar states are connected by $\{m_{001}|(1/2, 0)\}$ [23,41,42]. We assume such a symmetry operator $\hat{R}_{\rm BO} = \{R_{\rm BO}|\tau_{\rm BO}\}$ exists, i.e., $\hat{R}_{\rm BO}B_1 = B_2$. Here, $\tau_{\rm BO}$ represents an in-plane translation, and $R_{\rm BO}$ is one of the following seven types of symmetry operators allowed in 2D systems: (i) identity E; (ii) out-of-plane rotations; (iii)

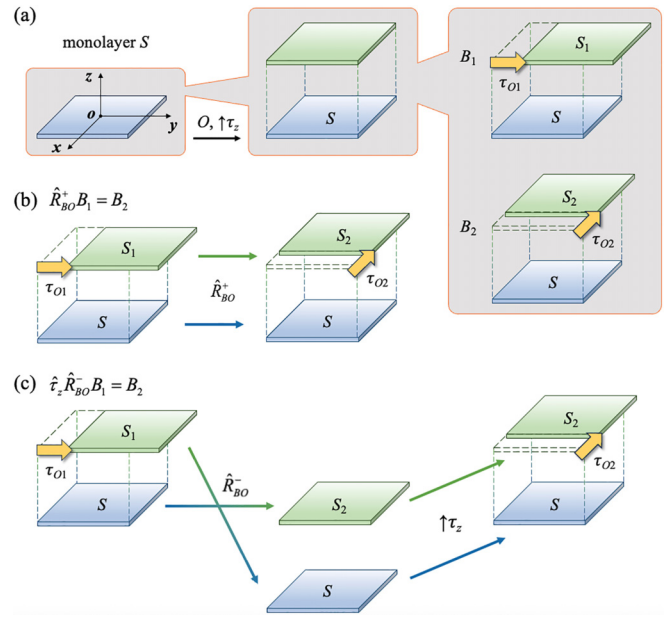

FIG. 4. (a) Formation of two energetically degenerate polar bilayers with different in-plane translations of τ_{O1} and τ_{O2}. The origin of the coordinate system ($\boldsymbol{o}$) is set on the bottom layer S. (b) Effect of $\hat{R}^{+}_{\rm BO}$ on connecting B_1 and B_2. Acting $\hat{R}^{+}_{\rm BO}$ on B_1 to obtain B_2 is equal to transforming S_1 into S_2, and S into itself. (c) Effect of $\hat{R}^{-}_{\rm BO}$ on connecting B_1 and B_2. Acting $\hat{R}^{-}_{\rm BO}$ on B_1 to obtain B_2 is equal to transforming S_1 into S, and S into S_2. $\hat{\tau}_z = \{E|\tau_z\}$ is used to ensure that the coordinate origin remains on the bottom layer S.

vertical mirror planes; (iv) inversion I; (v) in-plane twofold rotations; (vi) horizontal mirror plane; and (vii) out-of-plane improper rotations. These seven symmetry operators can be classified into two categories based on whether they invert the z coordinates of atoms: R^+ (types i–iii) and R^- (types iv–vii). Next, we discuss the relationship between B_1 and B_2 in two cases, namely $\hat{R}_{\rm BO} = \hat{R}^+$ ($R_{\rm BO} = R^+$) and $\hat{R}_{\rm BO} = \hat{R}^-$ ($R_{\rm BO} = R^-$).

a. $\hat{R}_{\rm BO} = \hat{R}^+$. Since $\hat{R}^+$ preserves the z coordinates of atoms, it does not exchange the stacking order of the top and bottom layers. As shown in Fig. 4(b), for $\hat{R}_{\rm BO} = \hat{R}^+_{\rm BO} = \{R^+_{\rm BO}|\tau^+_{\rm BO}\}$, the equation $\hat{R}^+_{\rm BO}B_1 = B_2$ can be expressed in the following equivalent form:

$$\begin{aligned}\hat{R}^+_{\rm BO}B_1 = B_2 &\leftrightarrow R^+_{\rm BO}B_1 + \tau^+_{\rm BO} \\ &= B_2 \leftrightarrow \begin{cases} R^+_{\rm BO}S_1 + \tau^+_{\rm BO} = S_2 \\ R^+_{\rm BO}S + \tau^+_{\rm BO} = S \end{cases}. \end{aligned} \tag{2}$$

The second line of Eq. (2) indicates that $\hat{R}^+_{\rm BO}$ must belong to the LG of S, i.e., G_S. Substituting Eq. (1) into the first line of Eq. (2) gives

$$\begin{aligned} &R^+_{\rm BO}(OS + \tau_z + \tau_{O1}) + \tau^+_{\rm BO} = OS + \tau_z + \tau_{O2} \\ &\leftrightarrow R^+_{\rm BO}(OS + \tau_{O1}) + \tau^+_{\rm BO} = OS + \tau_{O2} \\ &\leftrightarrow O^{-1}R^+_{\rm BO}OS + O^{-1}R^+_{\rm BO}\tau_{O1} + O^{-1}\tau^+_{\rm BO} - O^{-1}\tau_{O2} = S. \end{aligned} \tag{3}$$

We set

$$\begin{aligned} O^{-1}R^+_{\rm BO}O &= R^+_{S1} \\ O^{-1}R^+_{\rm BO}\tau_{O1} + O^{-1}\tau^+_{\rm BO} - O^{-1}\tau_{O2} &= \tau^+_{S1}, \end{aligned} \tag{4}$$

then Eq. (3) can be rewritten as $R^+_{S1}S + \tau^+_{S1} = S \leftrightarrow \{R^+_{S1}|\tau^+_{S1}\} \in G_S$. This explains the meaning of the first line of Eq. (4) that if $\hat{R}^+_{\rm BO}B_1 = B_2$, then $R^+_{\rm BO}$ and all elements in its conjugacy class must belong to G_{S0}. For clarity, we have listed all conjugacy classes of the D_{4h} and D_{6h} PGs for 2D systems in the Sec. II of the Supplemental Material [44]. For the second line of Eq. (4), multiplying both sides by O yields the relationship between τ_{O1} and τ_{O2}:

$$R^+_{\rm BO}\tau_{O1} + \tau^+_{\rm BO} - \tau_{O2} = O\tau^+_{S1}. \tag{5}$$

b. $\hat{R}_{\rm BO} = \hat{R}^-$. Since $\hat{R}^-$ reverses the sign of the z coordinates, it exchanges the stacking order of the top and bottom layers. As illustrated in Fig. 4(c), for $\hat{R}_{\rm BO} = \hat{R}^-_{\rm BO} = \{R^-_{\rm BO}|\tau^-_{\rm BO}\}$, the equation $\hat{R}^-_{\rm BO}B_1 = B_2$ can be expressed in the following equivalent form:

$$\begin{aligned}\hat{\tau}_z\hat{R}^-_{\rm BO}B_1 = B_2 &\leftrightarrow R^-_{\rm BO}B_1 + \tau_z + \tau^-_{\rm BO} \\ &= B_2 \leftrightarrow \begin{cases} R^-_{\rm BO}S_1 + \tau_z + \tau^-_{\rm BO} = S \\ R^-_{\rm BO}S + \tau_z + \tau^-_{\rm BO} = S_2 \end{cases}. \end{aligned} \tag{6}$$

Note that when $\hat{R}^-_{\rm BO}$ is acting on the bilayer system, it requires an additional out-of-plane translation $\hat{\tau}_z = \{E|\tau_z\}$ to ensure that the origin coordinate system ($\boldsymbol{o}$) remains at the bottom layer. By comparing the second lines of Eqs. (1) and (6), we obtain

$$\begin{aligned} R^-_{\rm BO}S + \tau_z + \tau^-_{\rm BO} = S_2 \\ OS + \tau_z + \tau_{O2} = S_2 \end{aligned} \rightarrow \begin{cases} R^-_{\rm BO} = O \\ \tau^-_{\rm BO} = \tau_{O2} \end{cases}, \tag{7}$$

which indicates that if $\hat{\tau}_z\hat{R}^-_{\rm BO}B_1 = B_2$, then $\hat{R}^-_{\rm BO}$ must be equal to the operator $\hat{O}_2 = \{O|\tau_{O2}\}$ that forms B_2. Substituting the first line of Eq. (1) into the first line of Eq. (6) gives

$$\begin{aligned} &R^-_{\rm BO}(OS + \tau_z + \tau_{O1}) + \tau_z + \tau^-_{\rm BO} = S \\ &\overset{R^-_{\rm BO}\tau_z = -\tau_z}{\longleftrightarrow} R^-_{\rm BO}OS + R^-_{\rm BO}\tau_{O1} + \tau^-_{\rm BO} = S \\ &\overset{\text{Eq.(7)}}{\longleftrightarrow} (R^-_{\rm BO})^2 S + R^-_{\rm BO}\tau_{O1} + \tau_{O2} = S. \end{aligned} \tag{8}$$

This shows that if $\hat{\tau}_z\hat{R}^-_{\rm BO}B_1 = B_2$, the following conditions must be satisfied:

$$(R^-_{\rm BO})^2 = R^+_{S2}, \tag{9}$$

$$R^-_{\rm BO}\tau_{O1} + \tau_{O2} = \tau^+_{S2}. \tag{10}$$

Here, $\{R^+_{S2}|\tau^+_{S2}\} \in G_S$. The subscripts "1" and "2" in $\hat{R}^+_{S1}$ and $\hat{R}^+_{S2}$ are only used to distinguish these two operators, which can be the same or different.

Now, we have presented the relationships between B_1 and B_2 for the two cases of $\hat{R}_{\rm BO} = \hat{R}^+$ and $\hat{R}_{\rm BO} = \hat{R}^-$, as expressed in Eqs. (5) and (10). When $\tau_{O1} = \tau_{O2}$, B_1 and B_2 represent the same bilayer stacking. In this case, Eqs. (4) and (5) and Eqs. (9) and (10) reduce to Eqs. (5)–(12) in the Supplemental Material of Ref. [26]. This serves as a validation of the reliability of our theoretical derivations. Furthermore, for symmorphic LGs, Eqs. (5) and (10) can be simplified to a more concise form:

$$R^\pm_{\rm BO}\tau_{O1} = \pm\tau_{O2}. \tag{11}$$

2. Workflow for determining the symmetry relations in stacked bilayers

Based on the above analysis, we investigate the ferroelectric switching behavior for all stacked polar bilayers. Since $R_{\rm BO}$ can be conveniently determined by Eqs. (4) and (9), we begin with B_1 and all possible $\hat{R}_{\rm BO}$ for it. By applying a specific $\hat{R}_{\rm BO}$ on B_1, the bilayer that is energetically degenerate with B_1 can be obtained, i.e., $B_i = \hat{R}_{\rm BO}B_1$. If $i = 1$, B_i is identical to B_1 itself; if $i \neq 1$, the obtained B_i represents a bilayer that differs from B_1 by an in-plane translation. According to $R_{\rm BO}$, the change of polarization direction between B_i and B_1 can be then determined.

In Fig. 5(a), we show the workflow for identifying the symmetry relationships and ferroelectric switching behaviors in bilayer systems. This method can be applied to all the 80 LGs. The workflow involves four steps: (i) Determine the in-plane translation τ_{O1} for a polar bilayer. (ii) Iterate over R^+ within G_{S0}; those satisfying $O^{-1}R^+O \in G_{S0}$ are $R^+_{\rm BO}$, and their corresponding translations in G_S are $\tau^+_{\rm BO}$. (iii) Iterate over R^- within C_O (the set containing O); those satisfying $(R^-)^2 \in G_{S0}$ are $R^-_{\rm BO}$, and their corresponding translations in G_S are $\tau^-_{\rm BO}$. (iv) Use Eqs. (5) and (10) to establish the correspondence between τ_{O1} and τ_{O2}, thereby determining the two bilayers B_1 and B_2 connected by $R^\pm_{\rm BO}$ as well as the change of polarization directions. Note that, as seen in steps (ii) and (iii), identifying all possible O is also crucial for studying ferroelectric switching behavior. We use *AB*- and *BA*-stacked bilayer BN with OP as an example to illustrate this process, which is presented in Fig. 5(b). For monolayer BN, G_S = LG-78,

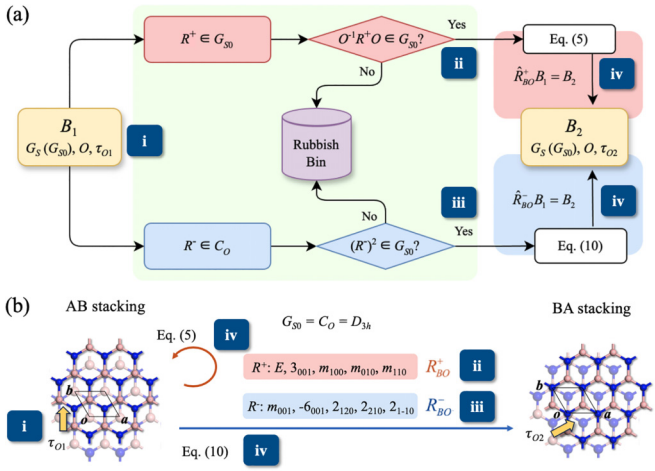

FIG. 5. (a) Workflow for identifying the symmetry relations in bilayer systems. Starting from a known bilayer B_1, the possible $\hat{R}_{\rm BO}$ can be identified to further determine the energy degenerate bilayer B_2. (b) Schematic diagram illustration the process for determining the symmetry relations between *AB*- and *BA*-stacked bilayer BN.

$G_{S0} = D_{3h}$. In bilayer BN, the two layers are related by pure translation, thus $C_O = G_{S0} = D_{3h}$, and O can be the identity operator E. (i) For *AB* stacking, $\tau_{O1} = (1/3,\ 2/3,\ 0)^T$. (ii) As $G_{S0} = D_{3h}$, $R^+ = 3_{001}$, m_{100}, m_{010}, and m_{110}, where each element can be $R^+_{\rm BO}$ as it satisfies $O^{-1}R^+O \in G_{S0}$. (iii) As $C_O = D_{3h}, R^- = m_{001}, 2_{120}, 2_{210}, 2_{1-10}$, and $-6^{\pm}_{001}$ where each element can be $R^-_{\rm BO}$ since it satisfies $(R^-)^2 \in G_{S0}$. (iv) According to Eq. (5), $R^+_{\rm BO}\tau_{O1} = (1/3, 2/3, 0)^T = \tau_{O1}$, indicating no energetically degenerate bilayer with a distinct configuration that can be related to *AB*-stacked BN through $R^+_{\rm BO}$. According to Eqs. (10) or (11), $R^-_{\rm BO}\tau_{O1} = (1/3, 2/3, 0)^T = -(2/3, 1/3, 0)^T = -\tau_{O2}$, which means that the *BA* stacking, characterized by in-plane translation τ_{O2}, can be related to *AB* stacking through one of these equivalent operators, i.e., m_{001}, 2_{120}, 2_{210}, 2_{1-10}, and $-6^{\pm}_{001}$. Since these operators reverse the z coordinates, the exchanged top and bottom layers will reverse the direction of polarization, consequently. This implies that bilayer BN exhibits OP ferroelectricity, which is in agreement with previous work [15–18,48,49].

3. *Overview of ferroelectric switching in stacked bilayer systems*

Using the workflow outlined above, we analyze and summarize the ferroelectric switching behavior of polar bilayers formed by stacking monolayers belonging to all 80 LGs (see Sec. III of the Supplemental Material [44]). Our results provide insight into understanding the absence of ferroelectricity in polar bilayer $PdSe_2$ as previously mentioned [Fig. 1(b)] (see Sec. IV of the Supplemental Material [44]). For systems exhibiting sliding ferroelectricity, we identify 12 distinct ferroelectric switching modes, as summarized in Table II. These modes are classified into three categories: single-component switching, nonsynchronous switching, and synchronous switching.

TABLE II. Twelve distinct switching modes for bilayer sliding ferroelectrics. The bilayer polarization types P_B include OP, IP, and CP. (↑↑) and (↑↓) represent the direction of OP unchanged and reversal, respectively, (0°) represents the direction of IP unchanged, and (60°, 90°, 120°, or 180°) refers to a rotation of IP with the corresponding angle.

P_B	Switching mode	LG (lattice type)	Categorization
OP	↑↓	3 (rC, hP), 6 ∼ 7 (rC, hP) 19 ∼ 21 (sP, hP), 22 (rC) 23 ∼ 25 (sP, hP) 37 ∼ 46 (sP, hP), 50, 59 60, 65 ∼ 69, 72, 74, 78	
IP	60°	73, 75, 76	single-component ferroelectric switching
	90°	23 ∼ 25 (sP), 37 ∼ 46 (sP) 49, 51 ∼ 54, 57 ∼ 60	
	120°	65 ∼ 72, 74, 78, 79	
	180°	3 (sP, hP), 6 ∼ 7 (rP, sP, hP) 19 ∼ 21 (rP, sP, hP) 23 ∼ 25 (hP), 27 ∼ 34 (rP, sP), 37 ∼ 46 (hP), 50	
CP	↑↓, 0°	14 ∼ 17 (rP, sP), 27 ∼ 34 (rP, sP, hP), 69 ∼ 72, 78, 79	non-synchronous ferroelectric switching
	↑↑, 60°	77	
	↑↑, 90°	55, 56	
	↑↑, 120°	69 ∼ 72, 78, 79	
	↑↑, 180°	23 ∼ 25 (rP, sP, hP) 37 ∼ 46 (sP), 57 ∼ 60	
	↑↓, 90°	23 ∼ 25 (sP) 37 ∼ 46 (sP), 57 ∼ 60	synchronous ferroelectric switching
	↑↓, 120°	69 ∼ 72, 78, 79	

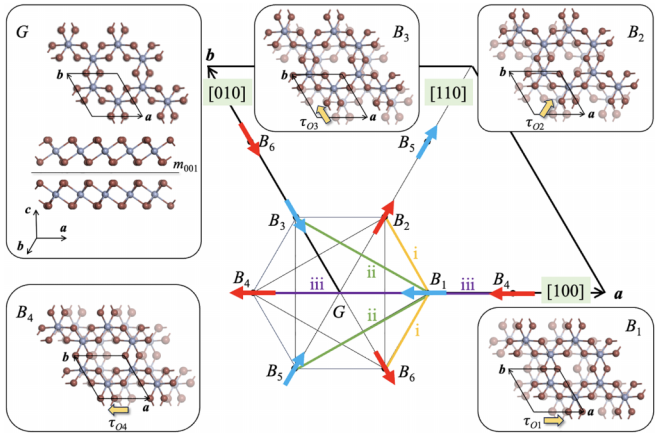

FIG. 6. B_1–B_6 are the six ground-state stacking points for bilayer CrI_3. All these bilayers exhibit CP with IP and OP components marked by arrows and color coding (red and blue), respectively. Yellow, green, and purple lines represent the three transition paths in polar bilayer CrI_3. The bilayer structures for direct stacking (G) and $B_1 - B_4$ stackings are also plotted.

Single-component switching occurs in the bilayers with pure OP or IP. For OP, interlayer sliding reverses polarization ($\uparrow\downarrow$), as observed in BN [16–18] and TMDs [19–22]. For IP, sliding may cause a 180° reversal or switches the direction of polarization by an angle of 60°, 90°, or 120°. Nonsynchronous switching in the bilayers with CP involves one component switching while the other remains unchanged, namely, OP flips ($\uparrow\downarrow$) while IP keeps unchanged (0°), or IP undergoes a rotation of 60°, 90°, 120°, or 180° while OP remains unchanged ($\uparrow\uparrow$). This behavior, characterized by independent switching of polarization components, could provide flexibility in the design of photoelectric devices [50]. Synchronous switching represents another intriguing category with both the directions of IP and OP changes simultaneously. Through the improved BSF theory, the ferroelectric switching in previously studied 2D CrI_3 [26] can be understood. The monolayer CrI_3 belongs to LG-71, and its bilayer with a flipped top layer ($O = m_{001}$) exhibits CP for six degenerate stackings $B_1 \sim B_6$ corresponding to interlayer translation points (1/3, 0), (1/3, 1/3), (0, 1/3), (−1/3, 0), (−1/3, −1/3), and (0, −1/3) [26] (Fig. 6). Our theory reveals that adjacent ground states are related by -6_{001}, satisfying $(-6^{+}_{001}) \cdot B_i = B_{i+1}$ $(i = 1 - 5)$ (see Sec. IV of the Supplemental Material [44]). Accordingly, there are three possible types of transition paths for bilayer CrI_3: (i) $B_1 \to B_2$ (B_6) via $-6^{\pm}_{001}$: OP flips ($\uparrow\downarrow$), while IP rotates 120° from [−100] to [110] (or [0-10]); (ii) $B_1 \to B_3$ (B_5) via $(-6^{\pm}_{001})^2 = 3^{\pm}_{001}$: OP remains unchanged ($\uparrow\uparrow$), while IP rotates 120° from [−100] to [0-10] (or [110]); (iii) $B_1 \to B_4$ via $(-6^{\pm}_{001})^3 = m_{001}$: OP flips ($\uparrow\downarrow$), while IP remaining unchanged (0°). The path (i) simultaneously changes the directions of both OP and IP, exhibiting the synchronous switching behavior. In contrast, paths (ii) and (iii) with only one polarization component switches correspond to the mode of nonsynchronous switching. These are consistent with the computational results [26], which can be directly obtained from our theory. The synchronous switching can also occur in 2D systems with the square lattice, where OP flips while IP rotates 90° (Table II). Notably, we find that it is impossible to involve a reversal of OP and a 180° rotation of IP at the same time, because such switching requires $R^{-}_{\mathrm{BO}} = I$. However, the bilayers connected by inversion are inherently nonpolar, hence ruling out this type of ferroelectric switching.

TABLE III. Possible multiple polar states of the bilayers obtained by stacking two monolayers.

No. of multiple polar states	LG (lattice type)
3	65 ∼ 68, 74
4	3 (rC), 6 ∼ 7 (rC), 13 (rC), 18 (rC), 22 (rC), 23 ∼ 25 (sP), 37 ∼ 46 (sP), 49, 51 ∼ 56, 57 ∼ 60
6	69 ∼ 73, 75 ∼ 79

In Fig. 6, an interesting phenomenon can be observed: the polarization directions of $B_1 - B_6$ are all different. This implies the existence of multiple polar states in this system, which contracts with the case of common bilayers, like BN with only two polar states. It can be also understood with our method. Starting from $\hat{R}_{\mathrm{BO}}B_1 = B_2$, if $(\hat{R}_{\mathrm{BO}})^2 \in G_S$, then applying $\hat{R}_{\mathrm{BO}}$ twice yields $(\hat{R}_{\mathrm{BO}})^2 B_1 = \hat{R}_{\mathrm{BO}}B_2 = B_1$, i.e., B_2 is mapped back to B_1, hence showing only two states. In contrast, if $(\hat{R}_{\mathrm{BO}})^2 \notin G_S$, like -6_{001} in CrI_3, the relation $(\hat{R}_{\mathrm{BO}})^2 B_1 = \hat{R}_{\mathrm{BO}}B_2$ does not transform B_2 to B_1, which leads to another new polar state. Table III summarizes the LGs, and the monolayers that are capable of forming more than two polar states. Note that multiple polar states in sliding ferroelectrics have been recently reported in multilayer stacks beyond bilayers, such as N-layer $3R$-MoS_2 [20,51], tetralayer graphene [52], and trilayer g-C_3N_4 [30]. Here, we demonstrate that this phenomenon can also occur in some bilayer systems. Due to the energy degeneracy, the magnitudes of polarization strength in such bilayers are identical, but their polarization directions are different, showing the "multidirectional" ferroelectricity. This discovery enhances the understanding of 2D vdW polar materials, and provides a strategy for the design of sliding ferroelectrics.

IV. CONCLUSIONS

In summary, to deepen the understanding and further improve the universality of BSF theory, we have carefully analyzed the limitations of the theory in the selection of rotation operators for the bilayers stacking of monolayers belonging to the oblique and rectangular crystal systems, and have proposed a more general method for identifying possible rotation operators. With this refinement, we have redriven the symmetry of the bilayer structures formed by stacking two monolayers belonging to these crystal systems, revealing more diverse polar states as compared to the original BSF theory. We have further developed a group theory framework to identify the symmetry relations in stacked bilayers. Building on this, the ferroelectric switching behavior is added to the BSF theory, enabling the prediction of potential ferroelectricity in stacked bilayers. In addition, we have demonstrated that multiple polar states can exist in some stacked bilayers. The

improved BSF theory is more general and more convenient for the design of sliding ferroelectrics for device applications.

ACKNOWLEDGMENTS

This work was supported by grants from the Fundamental Research Funds for the Central Universities (Grants No. 2024YJS193 and No. 2024XKRC056) and the National Natural Science Foundation of China (Grant No. 12104037).

DATA AVAILABILITY

The data that support the findings of this article are not publicly available. The data are available from the authors upon reasonable request.

[1] A. Belianinov, Q. He, A. Dziaugys, P. Maksymovych, E. Eliseev, A. Borisevich, A. Morozovska, J. Banys, Y. Vysochanskii, and S. V. Kalinin, $CuInP_2S_6$ room temperature layered ferroelectric, Nano Lett. **15**, 3808 (2015).

[2] F. Liu, L. You, K. L. Seyler, X. Li, P. Yu, J. Lin, X. Wang, J. Zhou, H. Wang, H. He *et al.*, Room-temperature ferroelectricity in $CuInP_2S_6$ ultrathin flakes, Nat. Commun. **7**, 12357 (2016).

[3] C. Cui, W.-J. Hu, X. Yan, C. Addiego, W. Gao, Y. Wang, Z. Wang, L. Li, Y. Cheng, P. Li *et al.*, Intercorrelated in-plane and out-of-plane ferroelectricity in ultrathin two-dimensional layered semiconductor In_2Se_3, Nano Lett. **18**, 1253 (2018).

[4] W. Ding, J. Zhu, Z. Wang, Y. Gao, D. Xiao, Y. Gu, Z. Zhang, and W. Zhu, Prediction of intrinsic two-dimensional ferroelectrics in In_2Se_3 and other III_2-VI_3 van der waals materials, Nat. Commun. **8**, 14956 (2017).

[5] Y. Zhou, D. Wu, Y. Zhu, Y. Cho, Q. He, X. Yang, K. Herrera, Z. Chu, Y. Han, M. C. Downer *et al.*, Out-of-plane piezoelectricity and ferroelectricity in layered α-In_2Se_3 nanoflakes, Nano Lett. **17**, 5508 (2017).

[6] J. Gou, H. Bai, X. Zhang, Y. L. Huang, S. Duan, A. Ariando, S. A. Yang, L. Chen, Y. Lu, and A. T. S. Wee, Two-dimensional ferroelectricity in a single-element bismuth monolayer, Nature (London) **617**, 67 (2023).

[7] S. Yuan, X. Luo, H. L. Chan, C. Xiao, Y. Dai, M. Xie, and J. Hao, Room-temperature ferroelectricity in $MoTe_2$ down to the atomic monolayer limit, Nat. Commun. **10**, 1775 (2019).

[8] J. A. Mundy, J. Schaab, Y. Kumagai, A. Cano, M. Stengel, I. P. Krug, D. M. Gottlob, H. Doğanay, M. E. Holtz, R. Held *et al.*, Functional electronic inversion layers at ferroelectric domain walls, Nat. Mater. **16**, 622 (2017).

[9] S. Wang, L. Liu, L. Gan, H. Chen, X. Hou, Y. Ding, S. Ma, D. W. Zhang, and P. Zhou, Two-dimensional ferroelectric channel transistors integrating ultra-fast memory and neural computing, Nat. Commun. **12**, 53 (2021).

[10] J. Xin and Y. Guo, Bulk photovoltaic effect in the elemental blue phosphorus-based polar homojunction and heterojunction, J. Phys. Chem. C **128**, 9705 (2024).

[11] Y. Li, J. Xin, Y. Guo, Z. Li, and X. Zhang, Ferroelectricity and nonlinear optical responses in two-dimensional distorted MX_2Y (M = Cu, Ag, Au; X = Chalcogens; Y = Halogen) monolayers, ACS Appl. Mater. Interfaces **17**, 6755 (2025).

[12] J. Xin, Y. Guo, and Q. Wang, Screening Two-dimensional pyroelectric materials based on pentagonal chains with large shift current, Phys. Rev. Mater. **7**, 074001 (2023).

[13] Y. Li, J. Fu, X. Mao, C. Chen, H. Liu, M. Gong, and H. Zeng, Enhanced bulk photovoltaic effect in two-dimensional ferroelectric $CuInP_2S_6$, Nat. Commun. **12**, 5896 (2021).

[14] T. Rangel, B. M. Fregoso, B. S. Mendoza, T. Morimoto, J. E. Moore, and J. B. Neaton, Large bulk photovoltaic effect and spontaneous polarization of single-layer monochalcogenides, Phys. Rev. Lett. **119**, 067402 (2017).

[15] L. Li and M. Wu, Binary compound bilayer and multilayer with vertical polarizations: Two-dimensional ferroelectrics, multiferroics, and nanogenerators, ACS Nano **11**, 6382 (2017).

[16] M. Vizner Stern, Y. Waschitz, W. Cao, I. Nevo, K. Watanabe, T. Taniguchi, E. Sela, M. Urbakh, O. Hod, and M. Ben Shalom, Interfacial ferroelectricity by van der Waals sliding, Science **372**, 1462 (2021).

[17] K. Yasuda, X. Wang, K. Watanabe, T. Taniguchi, and P. Jarillo-Herrero, Stacking-engineered ferroelectricity in bilayer boron nitride, Science **372**, 1458 (2021).

[18] K. Yasuda, E. Zalys-Geller, X. Wang, D. Bennett, S. S. Cheema, K. Watanabe, T. Taniguchi, E. Kaxiras, P. Jarillo-Herrero, and R. Ashoori, Ultrafast high-endurance memory based on sliding ferroelectrics, Science **385**, 53 (2024).

[19] R. Bian, R. He, E. Pan, Z. Li, G. Cao, P. Meng, J. Chen, Q. Liu, Z. Zhong, W. Li *et al.*, Developing fatigue-resistant ferroelectrics using interlayer sliding switching, Science **385**, 57 (2024).

[20] P. Meng, Y. Wu, R. Bian, E. Pan, B. Dong, X. Zhao, J. Chen, L. Wu, Y. Sun, Q. Fu *et al.*, Sliding induced multiple polarization states in two-dimensional ferroelectrics, Nat. Commun. **13**, 7696 (2022).

[21] X. Li, B. Qin, Y. Wang, Y. Xi, Z. Huang, M. Zhao, Y. Peng, Z. Chen, Z. Pan, J. Zhu *et al.*, Sliding ferroelectric memories and synapses based on rhombohedral-stacked bilayer MoS_2, Nat. Commun. **15**, 10921 (2024).

[22] X. Wang, K. Yasuda, Y. Zhang, S. Liu, K. Watanabe, T. Taniguchi, J. Hone, L. Fu, and P. Jarillo-Herrero, Interfacial ferroelectricity in rhombohedral-stacked bilayer transition metal dichalcogenides, Nat. Nanotechnol. **17**, 367 (2022).

[23] Z. Fei, W. Zhao, T. A. Palomaki, B. Sun, M. K. Miller, Z. Zhao, J. Yan, X. Xu, and D. H. Cobden, Ferroelectric switching of a two-dimensional metal, Nature (London) **560**, 336 (2018).

[24] F. Sui, M. Jin, Y. Zhang, R. Qi, Y.-N. Wu, R. Huang, F. Yue, and J. Chu, Sliding ferroelectricity in van der waals layered γ-InSe semiconductor, Nat. Commun. **14**, 36 (2023).

[25] Q. Liang, G. Zheng, S. Fan, L. Yang, and S. Zheng, Multidirectional sliding ferroelectricity of rhombohedral-stacked InSe for reconfigurable photovoltaics and imaging applications, Adv. Mater. **37**, 2416117 (2025).

[26] J. Ji, G. Yu, C. Xu, and H. J. Xiang, General theory for bilayer stacking ferroelectricity, Phys. Rev. Lett. **130**, 146801 (2023).

[27] H. Cheng, H. Chen, G. Hu, X. Yuan, J. Ren, and X. Zhao, Electrical control of the valley–layer hall effect in ferromagnetic bilayer lattices, J. Phys. Chem. Lett. **15**, 8759 (2024).

[28] D. Bennett, G. Martínez-Carracedo, X. He, J. Ferrer, P. Ghosez, R. Comin, and E. Kaxiras, Stacking-engineered ferroelectricity and multiferroic order in van der Waals magnets, Phys. Rev. Lett. **133**, 246703 (2024).

[29] L. Li, X. Li, L. Lin, D. Zhang, M. Chen, D. Wu, and Y. Yang, Sliding- and twist-tunable valley polarization in bilayer NiI_2, Phys. Rev. B **110**, 205119 (2024).

[30] Y. Wei, Z. Hu, X. Ma, H. Wang, F. Gao, X. Ma, Y. Wang, and W. Ren, In-plane sliding ferroelectricity and piezoelectricity in bilayer and trilayer g-C_3N_4, Phys. Rev. B **110**, 174103 (2024).

[31] J. Tan, D. Xu, M. Ge, G. Yang, and G. Ouyang, Sliding ferromagnetism in bilayer $MnSiSe_3$ and its application to spintronics, Phys. Rev. B **110**, 125402 (2024).

[32] S. Zeng and Y.-J. Zhao, Bilayer stacking A-type altermagnet: A general approach to generating two-dimensional altermagnetism, Phys. Rev. B **110**, 174410 (2024).

[33] C. Zhang, Z. Zhang, Z. Wu, X. Li, Y. Wu, and J. Kang, Modulation of polarization in sliding ferroelectrics by introducing intrinsic electric fields, J. Phys. Chem. Lett. **15**, 8049 (2024).

[34] L. Zhang, Y. Liu, M. Wu, and G. Gao, Electric-field- and stacking-tuned antiferromagnetic FeClF Bilayer: The coexistence of bipolar magnetic semiconductor and anomalous valley hall effect, Adv. Funct. Mater. **35**, 2417857 (2025).

[35] D. Campi, N. Mounet, M. Gibertini, G. Pizzi, and N. Marzari, Expansion of the materials cloud 2D database, ACS Nano **17**, 11268 (2023).

[36] A. D. Oyedele, S. Yang, L. Liang, A. A. Puretzky, K. Wang, J. Zhang, P. Yu, P. R. Pudasaini, A. W. Ghosh, Z. Liu *et al.*, $PdSe_2$: Pentagonal two-dimensional layers with high air stability for electronics, J. Am. Chem. Soc. **139**, 14090 (2017).

[37] G. Kresse and J. Furthmüller, Efficient iterative schemes for *ab initio* total-energy calculations using a plane-wave basis set, Phys. Rev. B **54**, 11169 (1996).

[38] P. E. Blöchl, Projector augmented-wave method, Phys. Rev. B **50**, 17953 (1994).

[39] J. P. Perdew, K. Burke, and M. Ernzerhof, Generalized gradient approximation made simple, Phys. Rev. Lett. **77**, 3865 (1996).

[40] H. J. Monkhorst and J. D. Pack, Special points for brillouin-zone integrations, Phys. Rev. B **13**, 5188 (1976).

[41] J. Xiao, Y. Wang, H. Wang, C. D. Pemmaraju, S. Wang, P. Muscher, E. J. Sie, C. M. Nyby, T. P. Devereaux, X. Qian *et al.*, Berry curvature memory through electrically driven stacking transitions, Nat. Phys. **16**, 1028 (2020).

[42] H. Wang and X. Qian, Ferroelectric nonlinear anomalous Hall effect in few-layer WTe_2, npj Comput. Mater. **5**, 1 (2019).

[43] A. M. Glazer, M. I. Aroyo, and A. Authier, Seitz symbols for crystallographic symmetry operations, Acta Crystallogr. Sect. A **70**, 300 (2014).

[44] See Supplemental Material at http://link.aps.org/supplemental/10.1103/PhysRevB.111.224102 for Seitz symbols, conjugacy classes for D_{4h} and D_{6h}, BSF for all 80 LGs within the improved theory, and BSF for $LiAuI_4$, $PdSe_2$, and CrI_3.

[45] D. B. Litvin and T. R. Wike, *Character Tables and Compatibility Relations of The Eighty Layer Groups and Seventeen Plane Groups* (Springer, Boston, MA, 1991).

[46] C. Kittel and P. McEuen, *Introduction to Solid State Physics* (John Wiley & Sons, New York, 2018).

[47] M. N. Gjerding, A. Taghizadeh, A. Rasmussen, S. Ali, F. Bertoldo, T. Deilmann, N. R. Knøsgaard, M. Kruse, A. H. Larsen, S. Manti *et al.*, Recent progress of the Computational 2D Materials Database (C2DB), 2D Mater. **8**, 044002 (2021).

[48] J. Wang, X. Li, X. Ma, L. Chen, J.-M. Liu, C.-G. Duan, J. Íñiguez-González, D. Wu, and Y. Yang, Ultrafast switching of sliding polarization and dynamical magnetic field in van der waals bilayers induced by light, Phys. Rev. Lett. **133**, 126801 (2024).

[49] Q. Yang and S. Meng, Light-induced complete reversal of ferroelectric polarization in sliding ferroelectrics, Phys. Rev. Lett. **133**, 136902 (2024).

[50] R.-C. Xiao, Y. Gao, H. Jiang, W. Gan, C. Zhang, and H. Li, Non-synchronous bulk photovoltaic effect in two-dimensional interlayer-sliding ferroelectrics, npj Comput. Mater. **8**, 1 (2022).

[51] S. Deb, W. Cao, N. Raab, K. Watanabe, T. Taniguchi, M. Goldstein, L. Kronik, M. Urbakh, O. Hod, and M. Ben Shalom, Cumulative polarization in conductive interfacial ferroelectrics, Nature (London) **612**, 465 (2022).

[52] L. Yang, S. Ding, J. Gao, and M. Wu, Atypical sliding and Moir'e ferroelectricity in pure multilayer graphene, Phys. Rev. Lett. **131**, 096801 (2023).